Computing
https://doi.org/10.1007/s00607-018-0678-6

An end-to-end joint learning framework of artery-specific coronary calcium scoring in non-contrast cardiac CT

Weiwei Zhang[1] · Jinglin Zhang[2] · Xiuquan Du[1] · Yanping Zhang[1] · Shuo Li[3]

Received: 16 October 2018 / Accepted: 9 November 2018

Abstract

Accurate identification and quantification of coronary artery calcification play an import role in early diagnosis of coronary heart disease and atherosclerosis. In this paper, we have proposed an end-to-end joint learning framework (CAC-Net) for artery-specific coronary calcification identification in non-contrast cardiac CT. Unlike the previous methods, the framework establish direct mapping relationship between input CT and calcification, consequently, it can directly yield accurate results based on the given CT scans in testing process. In this framework, the intra-slice calcification features are collected by an U-DenseNet module, which is the combination of Dense Convolutional Network (DenseNet) and U-Net. Subsequently, 3D U-Net is performed to extract the inter-slice calcification feature. Joint learning of 2D and 3D module brings rich semantic features, which are beneficial to artery-specific calcification identification. In our experiment, 169 non-contrast CT exams collected from two centers are used to validate the performance of our framework. By the cross validation, we have achieved a sensitivity of 0.905, a PPV of 0.966 for calcification number and a sensitivity of 0.933, a PPV of 0.960 and a F1 score of 0.946 for calcification volume, respectively. The intra-class correlation coefficient are 0.986 for Agatston score and 0.982 for volume score. The quantitative results indicate that our method can be used as a reliable clinical diagnostic tool for coronary calcification identification.

Keywords Coronary artery calcification · Joint learning · End-to-end

Mathematics Subject Classification 92C55 (Biomedical imaging and signal processing)

✉ Xiuquan Du
dxqllp@163.com

1 School of Computer Science and Technology, Anhui University, Hefei, Anhui, China

2 School of Atmospheric Sciences, Nanjing University of Information Science and Technology, Nanjing, Jiangsu, China

3 Department of Medical Imaging, Western University, London, ON, Canada

Published online: 16 November 2018

1 Introduction

The amount of coronary artery calcification (CAC) has been widely used as an indicator of cardiovascular disease (CVD) [1]. In clinical practice, CAC in left main (LM), left anterior descending (LAD), left circumflex (LCX) and right coronary artery (RCA) are routinely located by physicians manually in non-contrast-enhanced ECG-triggered cardiac calcium scoring CT (CSCT). After obtaining CAC lesions, the coronary artery calcium score (CACS), which is commonly used to express the amount of CAC, is subsequently calculated by commercially available software. Manual identification of CAC is an uncomplicated and repeated task, but it is a time-consuming and inefficient procedure in clinical diagnosis. Furthermore, the manual identification method might not be practical in near future because of the largely increasing cardiac CT exams as indicated by Goff et al. [2]. In recent years, a number of computer-aided CAC identification methods have been proposed to compute the coronary artery calcium score. These methods involved in non-contrast cardiac CT, contrast enhanced cardiac CT angiography (CTA) and non-contrast chest CT [3–7]. Also, rapidly developing deep learning technique is used for the calcification identification domain [8–12]. Compared to manual method, these automatic or semi-automatic methods not only reduce workload of experts in CVD research, but also improve efficiency in clinical diagnostic procedure.

However, the previous automatic and semi-automatic CAC identification methods have several limitations in clinical practice. In terms of anatomical structure, CAC lesions have uncertain position and diverse structure. Moreover, identification of CAC lesions suffer from the interference of tissues with similar intensity, such as rib and spine. Consequently, earlier identification methods routinely delimit region of interest (ROI) by different algorithms to reduce interference. In addition, the previous CAC identification methods always divide into two steps: obtaining candidate CAC lesions and candidate lesions classification [11–13]. Such indirect mapping relationship give rise to the greater possibility of losing useful CAC information in CT image because of the complicated information delivery process. And, in the classification step of these methods, available hand-rafted features described candidate lesions are extracted by the corresponding feature extraction algorithms [13–15]. As a result, either the features may not comprehensively describe CAC lesions, or redundant information is generated inevitably. Moreover, the classification step just focus on CAC lesions. It can not fully make use of the prior information of relationships among different arteries.

In this work, we have proposed an end-to-end deep learning framework using joint representation of intra-slice and inter-slice CAC features for CAC identification [16]. The framework has several remarkable characteristics. Specifically, the proposed framework need no additional pre-processing procedure to obtain ROI area. It directly takes the original non-contrast cardiac CT image as input. Furthermore, the proposed framework is an end-to-end system, thus, it avoids the error propagation or accumulation from obtaining candidate CAC lesions step to candidate lesions classification step of previous methods. Compared with earlier two-step methods, our framework establishes direct mapping relationship between the CT image and CAC identification. In the framework, rich artery-specific automatic features are learned to replace hand-rafted lesion features used in earlier methods. The framework makes use of the

tightly-coupled modified 2D DenseNet and 3D U-Net to learn the hierarchical intra-slice feature and volumetric contexts respectively. The adopted deep network not only tackle the problem of 2D operation neglecting volumetric contexts, but also prevents the heavy computational cost existed in 3D operation. When the two sub-network are trained jointly, the framework not only enhance expressiveness of image representation, but also extract rich available semantic features about CAC. Moreover, the proposed framework takes CAC identification problem as a artery-specific multi-class classification task. In terms of anatomical structure, different arteries are interconnected, including LM, LAD and LCX. Therefore, the multi-class classification task can fully uses the correlation relationship among multiple arteries. As with Wolterink's point, we also consider calcification distributed in LM and LAD as LAD calcification [14].

2 Methodology

In this work, we have proposed a integrated framework CAC-Net for coronary artery calcification (CAC) identification, as shown in Fig. 1. By the input non-contrast cardiac CT images, CAC-Net applies a 2D U-DenseNet module to extract intra-slice calcification feature. Because the most calcification lesions span multiple adjacent image slices, the CAC-Net applies a 3D U-Net module to extract inter-slice calcification feature. These two feature modules are detailed in Sects. 2.1 and 2.2, respectively. Following the feature extraction architecture, a softmax layer is used for artery-specific calcification classification.

2.1 Intra-slice feature extraction with 2D U-DenseNet

Our framework extracts the intra-slice calcification feature by a 2D U-DenseNet module, which is extended by the structures of DenseNet [17]. The U-DenseNet has several improvements compared to DenseNet and U-Net in generalizability, information delivery and computational cost [17,18]. In our work, the calcification identification task is considered as a semantic segmentation problem. Consequently, our U-DenseNet treats the basic DenseNet architecture as the contracting path of feature extraction, and subsequently add the corresponding expanding path to get original size feature map. The number of dense blocks in contracting path and expanding path is same. And the number of layers in same-level blocks is also same. The similar devised architectures were proposed in recent works [19]. Inspired by the skip connections of U-Net, the expanding path of U-DenseNet preserves the same-level information from contracting path to neglect possible information loss caused by pooling and deconvolution operations [18]. As a result, U-DenseNet is more efficient for segmentation task than the network without skip connections. Recent works indicated that addition operation between feature maps does not lead to much performance loss compared to concatenation, but it can significantly reduce the computational load. So for the skip connections between contracting path and expanding path in U-DenseNet, the summation between same-level feature maps is used to replace the concatenation operation of U-Net.

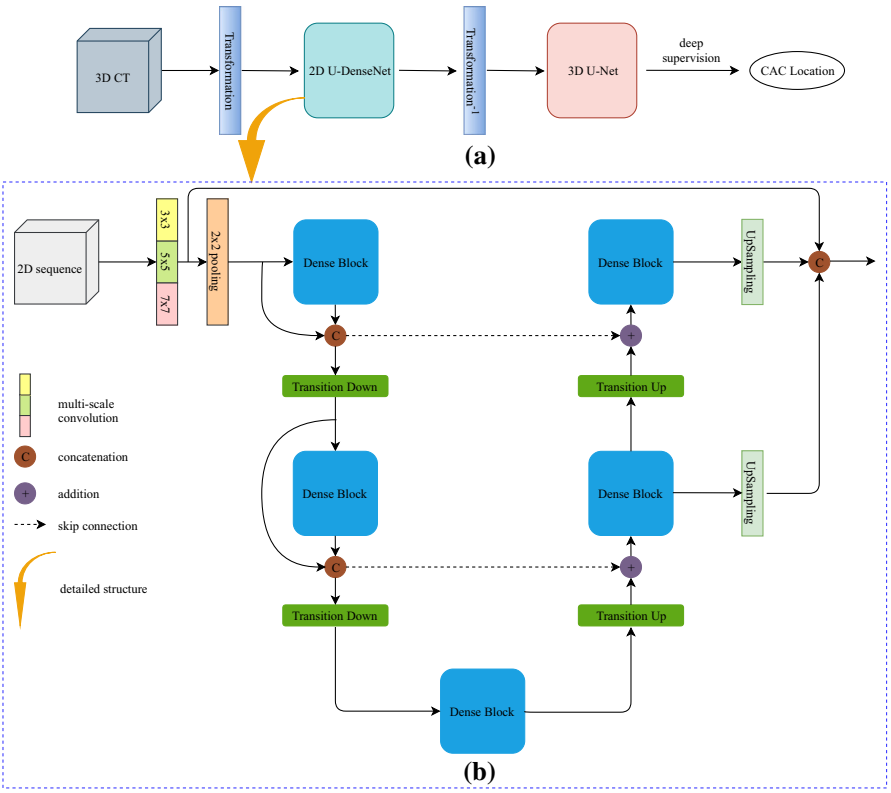

Fig. 1 **a** Flow chart of the proposed framework. **b** Detailed structure of the 2D U-DenseNet. See Sect. 2 for the exhaustive structure explanation

The detailed structure of U-DenseNet is shown in Fig. 1b. For the input of U-DenseNet, We apply multi-scale convolution operation (kernel size: 3×3, 5×5, 7×7) to capture multi-scale contextual information and interrelation among multiple structures. U-DenseNet has three downwards dense blocks, three upwards dense blocks and one bottleneck block. The number of conv-blocks in these dense blocks are 3, 4, 5, 6, 5, 4, 3, respectively. Each conv-block consists of a series of batch normalization (BN), 1×1 convolution (conv), rectified linear unit (ReLu), BN, 3×3 conv, ReLu in a sequence. In contracting path, a transition down (TD) layer is used after every dense block to reduce the size of feature map. Each TD layer consisted of a series of BN, ReLu, 1×1 conv, 2×2 max pooling layer. The input of every TD layer is the concatenation of the input and output of adjacent preceding block. In expanding path, to reduce the parameters size, U-DenseNet takes the output of bottleneck block as initial input of expanding path, no longer cascading the input of this block. U-DenseNet adds a transition up (TU) layer, i.e. a bilinear interpolation operation, before every upwards dense blocks to expand the size of feature map. For each block, its input is the summation of the outputs of adjacent TU layer and same-level dense block in contracting path. Before the addition operation, the feature map of same-level block is

subjected to a 1x1 convolution to make channels of the two objects same. Besides, the summation of input and output of every block is used as input of the next TU layer. To prevent over-fitting, U-DenseNet applies the dropout operation after every convolution. Droput rate is set to 0.5. To fully take advantage of the multi-level information in U-DenseNet module, the outputs of all blocks in expanding path are cascaded as input of the subsequent 3D module.

2.2 Inter-slice feature extraction with deformed 3D U-Net

Our framework extracts the inter-slice calcification feature by 3D U-Net module, which is deformed by 2D U-net architecture of Ronneberger et al. [18]. This module comprises a contracting path and a expansive path. In the contracting path, each sub-module consists of two $3 \times 3 \times 3$ convolution and a $2 \times 2 \times 2$ max pooling. Each convolution is followed by a group normalization (GN), ReLu and a dropout. Group normalization (GN) is used in each sub-module to speed up the training process [20]. And pooling operations facilitate 3D module to extract multi-level information. The number of feature map in each sub-module is twice the previous one. Such sub-module is repeated five times throughout the contracting path. Relatively, in the expansive path, each sub-module consists of a bilinear interpolation operation, a concatenation, two $3 \times 3 \times 3$ convolution. The bilinear interpolation is applied for up-sampling function to recover original image size, similarly to deconvolution layer of U-Net. Besides, the CAC-Net adds deep supervision mechanism on multi-level sub-modules for fast training and better performance of network. In total, the entire 3D feature module consists of 26 convlutional layers.

2.3 Joint representation of different feature modules

The 2D U-DenseNet extracts the representative and discriminative intra-slice calcification features, but it is incompetent for 3D context calcification features. For the subjects with high risk category, calcification lesions always span multiple adjacent slices. However, it is difficult for the pure 3D deep networks to extend its depth and width due to the GPU memory limitation. Consequently, we combine the 2D U-DenseNet module and 3D U-Net to extract comprehensive calcification features.

The well performance of the proposed framework comes from the joint representation of intra-slice CAC feature and inter-slice CAC feature. The joint representation and seamless connection of 2D U-DenseNet feature module and deformed 3D U-Net feature module are realized by a transformation operation before each module. Let $I \in R^{n \times W \times H \times D \times 1}$ denotes input of the proposed CAC-Net, $L_{CAC} \in R^{n \times W \times H \times D \times 4}$ (4 represents LAD, LCX, RCA, Total calcification) denotes CAC labels. To input 3D CT image to 2D U-DenseNet, function τ is used to convert 3D CT to 2D sequence CT, as described in

$$I_{2d\_input} = \tau(I) \tag{1}$$

where $I_{2d\_input} \in R^{(n \times D) \times W \times H \times 1}$ denotes the input of 2D U-DenseNet. To seamlessly combine 2D U-DenseNet module with the subsequent 3D network counterpart,

the inverse function τ^{-1} is used to convert 2D sequence back to 3D shape, as described in

$$y_{3d\_input} = \tau^{-1}(y_{2d\_output}) \tag{2}$$

The output of 3D feature module $I_{3d\_output} \in R^{n\times W\times H\times D\times C'}$ is used as the ultimate CAC feature, followed by a 1x1 convolutional layer and a softmax layer for artery-specific CAC classification.

2.4 Loss function

To effectively train the networks, we used a multi-class dice loss function for the CAC identification task. It comes from the segmentation dice loss proposed by Milletari [21], which is used for two-class classification. In order to achieve artery-specific multi-class calcification classification, we improved the two-class dice loss to multi-class dice loss. The specific representation is as follows

$$D_m(\cdot) = \sum_{i}^{K}\left(1 - \frac{2\cdot\sum_j^N P_{i,j}G_{i,j} + smooth}{\sum_j^N P_{i,j}^2 + \sum_j^N G_{i,j}^2 + smooth}\right) \tag{3}$$

where K denotes the number of calcification category, N denotes the number of voxels in each CT volume. $P_{i,j}$, $G_{i,j}$ denote the predicted and ground truth map of class i, respectively. $smooth$ as the smoothing term enables the gradients of all samples to be back propagated. To efficiently and quickly train the network, we add deep supervision mechanism on 3D feature module. Consequently, the objective function of entire network is written as

$$L = min\sum_{t}^{M} W_t D_m\left(P\left(X, W, t\right), G\right) + \lambda R\left(W\right) \tag{4}$$

where $X \in R$ is a 3D CT subject, $t \in M$ denotes task t in deep supervision mechanism, $D_m(\cdot)$ represents the loss of predicted $P(\cdot)$ and ground truth G, W_t is the weight of loss of each task and $R(W)$ denotes the regularization of W. L ranges between 0 and K, depending on the size of K.

3 Experiments and results

3.1 Materials acquisition

The proposed framework is evaluated by consecutive scanning non-contrast cardiac CT exams provided by Beijing Anzhen Hospital, Capital Medical University, Beijing, China. Patients are scanned by a multi-detector CT scanner and subsequent acquisitions are synchronized by ECG-triggering at 70% of the $R-R$ interval. In the scanning process, standard calcium scoring scanning protocol and 120 kVp tube voltage are adopted. Available CSCT images are acquired with a in-plane resolution of

0.3×0.3–0.5×0.5 mm^2 and a section thickness of 2.5 mm. The abnormal exams are discarded, including exams with consecutive repeat scanning, fewer scanning slices, high level of disturbance, anatomical abnormalities and metal implants such as intracoronary stents. Total 129 exams are obtained, all of which are between 18 and 83 years old, with an average age of 53.

In our work, the reference standard for CAC in provided exams comes from the consensus annotations of two experienced radiologists in CAC scoring (one has experience of annotations $>$ 2000 CSCT scans, another has experience of annotations $>$ 1500 CSCT scans). The basic annotation standard is that Hounsfield unit (HU) greater than 130 and lesion volume greater than 1.5 mm^3 by 6-connected components [22]. Each radiologist independently identifies all artery-specific CAC lesions and labels them according to above-mentioned annotation standard. Two radiologists compares their annotations. Subsequently, the reference standard of artery-specific CAC is obtained after consensus.

We evaluate performance of our framework based on the dataset by 5-fold cross validation. Each subject is assigned a cardiovascular risk category. Consequently, each test set covers all risk categories of exams. Subsequently, we also validate our framework on the dataset of 40 scans of orScore challenge [22]. To speed up the training process and improve network performance, the CT volumes are normalized to [0 1] by the min–max normalization. Test CT volumes are also normalized in the same way.

3.2 Evaluation metrics

The proposed framework is evaluated with several evaluation metrics of calcification based on the automatic detection results and manual consensus CAC labels. First, the performance of patient-specific CAC identification is quantified by the number and the volume of total calcifications [23]. Indicator sensitivity, positive predictive value (PPV) and F1 score are used for these performance valuation terms [22]. Second, the performance of artery-specific CAC identification is quantified by the agreement between reference and automatic CAC volume. The agreement is expressed by the absolute agreement two-way intra-class correlation coefficient (ICC), in which the confidence level defaults to 95%. Third, total CAC volume and Agatston score per subject are evaluated by ICC between automatic and manual labels [14].

3.3 Performance evaluation

In the section, performance on the two datasets is present via patient-specific CAC identification, artery-specific CAC identification and comparison with other methods.

First, we evaluate the performance of patient-specific CAC identification. Main experiment is implemented based on our dataset of 129 scans. The qualitative results indicate that our CAC-Net achieves well performance in CAC detection. Quantitative performance of patient-specific CAC identification is present vi sensitivity, PPV and F1 score. As indicated in Table 1, F1 score of our CAC-Net about CAC volume is

Table 1 Patient-specific performance of CAC-Net in terms of sensitivity, PPV and F1 score

Method	Sensitivity	PPV	F1 score
CAC number	0.905	0.966	0.935
CAC volume	0.933	0.960	0.946

Table 2 Artery-specific performance of CAC-Net in terms of ICC of Agatston, volume score

Scores	LAD	LCX	RCA	Patient
Agatston score	0.981	0.979	0.971	0.986
Volume score	0.980	0.978	0.968	0.982

Table 3 Comparison with other methods. Sen. represents sensitivity of total calcification number, and F1 score represents F1 score of total calcification volume

Methods	Interaction	Dataset	ICC	Sen.	F1 score
Kurkure et al. [13]	Automatic	CT (105)	–	0.921	–
Išgum et al. [24]	Automatic	CT (76)	–	0.738	–
Brunner et al. [25]	Automatic	CT (30)	–	0.863	–
Shahzad et al. [26]	Automatic	CT (157)	–	0.839	–
Proposed CAC-Net	Automatic	CT (129)	0.986	0.905	0.946
Shahzad et al.	Automatic	CT + CTA (40)	0.971	0.621	0.893
Durlak et al.	Automatic	CT (40)	0.989	0.835	0.951
Wolterink et al.	Automatic	CT (40)	0.986	0.845	0.947
Yange et al.	Semi-automatic	CT + CTA (40)	0.992	0.940	0.968
Kelm et al.	Automatic	CT + CTA (40)	0.980	0.838	0.943
Kondo et al.	Semi-automatic	CT + CTA (40)	0.621	0.513	0.623
Proposed CAC-Net	Automatic	CT (40)	0.991	0.911	0.954

0.946, which demonstrates that the proposed CAC-Net has reached convincing level in detection of CAC and non-calcification.

Second, we evaluate the performance of artery-specific CAC identification in terms of ICC. As shown in Table 2, ICC of volume scores for LAD, LCX, RCA are 0.980, 0.978, 0.968, respectively. The results effectively demonstrate the performance of our CAC-Net for per artery calcification in clinical indicator.

Third, we compare our CAC-Net with several previous methods indirectly in the five rows of Table 3. Even though these results can not be compared directly due to different dataset and different evaluation criteria, they present the differences of these methods. Subsequently, we compare our CAC-Net with methods of orScore challenge in the last seven rows of Table 3. These methods are based on same dataset and same evaluation criteria [22]. Consequently, the comparison of them can intuitively demonstrate the advantages of our framework.

Finally, we compare our CAC-Net with itself based on our dataset. As shown in Table 4, we use 3D FCN, 3D U-Net, our 2D U-DenseNet, and Twoflod U-Net (2D U-Net + 3D U-Net) for ablation experiments. The listed results demonstrate our CAC-

Table 4 Performance of ablation experiments. num is the abbreviation of calcification number and vol is the abbreviation of calcification volume

Structures	Sen. (num)	Sen. (vol)	PPV (num)	PPV (vol)	F1 score (vol)
FCN	0.860	0.875	0.915	0.912	0.893
U-Net	0.870	0.895	0.933	0.923	0.909
U-DenseNet	0.892	0.930	0.954	0.949	0.939
Twofold U-Net	0.895	0.928	0.942	0.940	0.934
CAC-Net	0.905	0.933	0.966	0.960	0.946

Net is reasonable and superior in network structure by the union of 2D U-DenseNet and 3D U-Net.

4 Discussion and analysis

Based on the coronary artery calcification detection task, we have proposed an automatic artery-specific calcification detection approach. The approach presents an automatic and end-to-end idea about calcification detection. For this proposed framework, it does not need the automatic or manual location of ROI, which is generally heart. In the previous methods, the ROI location algorithm usually requires independent and complex research. And these location algorithms can not exactly exclude the high level interference, such as spine, ribs, aorta, etc. However, the accuracy of ROI location directly affects the performance of calcification detection. Relatively speaking, our CAC-Net has no need of pre-processing procedure about ROI. It identifies the calcification by voxel-wise style instead of rough and fine classification of candidate lesions presented in previous methods. In the training process, it establishes the direct mapping relationship between input CT scans and corresponding calcification label. Also, it consider the artery-specific calcification detection task as a multiple classification problem.

The framework has been validated on our dataset of 129 CSCT scans and orScore dataset of 40 CSCT scans. As indicated in Tables 1 and 2, our CAC-Net is demonstrated by the numerically excellent results. The framework performs voxel-wise classification by semantic segmentation technique [27]. It not only extracts the in-plane information, and also aggregates volumetric contexts. The well performance of our framework comes from the seamless combination of 2D feature module and 3D feature module, as detailed in Sect. 2.3. The 2D feature module (U-DenseNet) is used to achieve intra-slice calcification feature. It is based on the dense connection of DenseNet and the skip connection of U-Net. The rationality of U-DenseNet in structure has been validated by the performance of FC-DenseNet in semantic segmentation [19]. However, it neglects the 3D context information. Consequently, the subsequent 3D U-Net is used to extract inter-slice calcification feature. With the guidance of U-DenseNet, 3D feature module performs quick and effective training and can be trend to thinner. CAC-Net has less parameters than pure 3D deep network, and the latter can not extend its depth and width for the GPU memory limitation. Pure 3D network is no longer used by researchers,

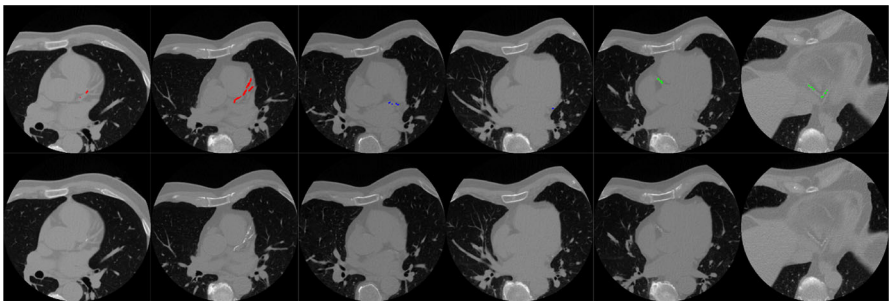

Fig. 2 Visual identification of a subject based on our framework. The first row presents the automatic results, and the second row present corresponding input slices. Calcification of LAD, LCX and RCA are denoted by red, blue and green areas, respectively (color figure online)

instead of the assemble of 3D network and other structures. In our work, the joint combination of 2D and 3D network bring the superior results of calcification detection.

The evaluation F1 score of CAC number (0.935) in Table 1 quantitatively describes that CAC-Net can identify the most of calcification lesions. And F1 score of CAC volume (0.946) and Fig. 2 indicates the precision of intra-lesion predication. This result also demonstrate that the effectiveness of CAC-Net in semantic segmentation. Table 4 shows the advantage of CAC-Net in structure. For U-Net and Twofold U-Net, the better performance of Twofold U-Net than U-Net comes from the joint representation of 2D feature and 3D feature. Independent U-DenseNet that only utilizes 2D contextual information has achieved similar performance due to the superiority of DenseNet [17]. Dense connection of U-DenseNet makes it has more richer calcification feature representations than U-Net. Consequently, the combination of U-DenseNet and U-Net, i.e. CAC-Net, has the best capability on calcification detection than U-DenseNet and Twofold U-Net.

5 Conclusion and recommendations

In this paper, we have proposed a joint learning framework for artery-specific coronary calcification automatic identification in non-contrast cardiac CT. The end-to-end framework establishes direct mapping relationship between input cardiac CT scans and corresponding calcification map based on the intra-slice and inter-slice features. It performs calcification identification voxel by voxel through semantic segmentation technique. Based on the given CT scans, the framework achieves F1 score of 0.935 in CAC number and 0.946 in CAC volume. The direct and indirect comparison with previous methods indicates that our method makes a little progress in coronary artery calcification identification domain. Consequently, our method can be consider as an effective clinical coronary artery calcification identification tool to aid radiologists. In the future, one key that should be explored is the potential performance of CAC-Net on contrast CTA because of the more and more CTA data in clinical practice. Another explored key is how to improve performance of the small object calcification detection. The CAC-Net does not show perfect performance on smaller lesions. Maybe,

multi-scale representation and generative adversarial network (GAN) have enough potential on this theme [28,29].

References

1. Yeboah J, McClelland RL, Polonsky TS, Burke GL, Sibley CT, OLeary D, Carr JJ, Goff DC, Greenland P, Herrington DM (2012) Comparison of novel risk markers for improvement in cardiovascular risk assessment in intermediate-risk individuals. Jama 308(8):788–795
2. Goff DC, Lloyd-Jones DM, Bennett G, Coady S, Dagostino RB, Gibbons R, Greenland P, Lackland DT, Levy D, ODonnell CJ et al (2014) 2013 acc/aha guideline on the assessment of cardiovascular risk: a report of the american college of cardiology/american heart association task force on practice guidelines. J Am Coll Cardiol 63(25):2935–2959
3. Mittal S, Zheng Y, Georgescu B, Vega-Higuera F, Zhou SK, Meer P, Comaniciu D (2010) Fast automatic detection of calcified coronary lesions in 3D cardiac CT images. In: International workshop on machine learning in medical imaging. Springer, pp 1–9
4. Priyatharshini R, Chitrakala S (2016) An active contour model based multi objective optimization technique for coronary calcium scoring. J Med Imaging Health Inf 6(7):1657–1662
5. Eilot D, Goldenberg R (2014) Fully automatic model-based calcium segmentation and scoring in coronary CT angiography. Int J Comput Assist Radiol Surg 9(4):595–608
6. Isgum I, Prokop M, Niemeijer M, Viergever MA, Van Ginneken B (2012) Automatic coronary calcium scoring in low-dose chest computed tomography. IEEE Trans Med Imaging 31(12):2322–2334
7. González G, Washko GR, Estépar RSJ (2016) Automated agatston score computation in a large dataset of non ECG-gated chest computed tomography. In: 2016 IEEE 13th international symposium on biomedical imaging (ISBI), IEEE, pp 53–57
8. Zhang J, Liu P, Zhang F, Song Q (2018) Cloudnet: ground-based cloud classification with deep convolutional neural network. Geophys Res Lett 45(16):8665–8672
9. Xue W, Islam A, Bhaduri M, Li S (2017) Direct multitype cardiac indices estimation via joint representation and regression learning. IEEE Trans Med Imaging 36(10):2057–2067
10. Wu S, Gao Z, Liu Z, Luo J, Zhang H, Li S (2018) Direct reconstruction of ultrasound elastography using an end-to-end deep neural network. In: International conference on medical image computing and computer-assisted intervention, Springer, pp 374–382
11. Wolterink JM, Leiner T, de Vos BD, van Hamersvelt RW, Viergever MA, Išgum I (2016) Automatic coronary artery calcium scoring in cardiac CT angiography using paired convolutional neural networks. Med Image Anal 34:123–136
12. Lessmann N, van Ginneken B, Zreik M, de Jong PA, de Vos BD, Viergever MA, Išgum I (2018) Automatic calcium scoring in low-dose chest CT using deep neural networks with dilated convolutions. IEEE Trans Med Imaging 37(2):615–625
13. Kurkure U, Chittajallu DR, Brunner G, Le YH, Kakadiaris IA (2010) A supervised classification-based method for coronary calcium detection in non-contrast CT. Int J Cardiovasc Imaging 26(7):817–828
14. Wolterink JM, Leiner T, Takx RA, Viergever MA, Išgum I (2015) Automatic coronary calcium scoring in non-contrast-enhanced ECG-triggered cardiac CT with ambiguity detection. IEEE Trans Med Imaging 34(9):1867–1878
15. Yang G, Chen Y, Ning X, Sun Q, Shu H, Coatrieux JL (2016) Automatic coronary calcium scoring using noncontrast and contrast CT images. Med Phys 43(5):2174–2186
16. Li X, Chen H, Qi X, Dou Q, Fu CW, Heng PA (2017) H-denseunet: Hybrid densely connected unet for liver and liver tumor segmentation from CT volumes. arXiv preprint arXiv:1709.07330
17. Huang G, Liu Z, Weinberger KQ, van der Maaten L (2017) Densely connected convolutional networks. In: Proceedings of the IEEE conference on computer vision and pattern recognition, vol 1, p 3
18. Ronneberger O, Fischer P, Brox T (2015) U-net: convolutional networks for biomedical image segmentation. In: International conference on medical image computing and computer-assisted intervention, Springer, pp 234–241
19. Jégou S, Drozdzal M, Vazquez D, Romero A, Bengio Y (2017) The one hundred layers tiramisu: Fully convolutional densenets for semantic segmentation. In: 2017 IEEE conference on computer vision and pattern recognition workshops (CVPRW), IEEE, pp 1175–1183
20. Wu Y, He K (2018) Group normalization. arXiv preprint arXiv:1803.08494

21. Milletari F, Navab N, Ahmadi SA (2016) V-net: Fully convolutional neural networks for volumetric medical image segmentation. In: 2016 fourth international conference on 3D vision (3DV), IEEE, pp 565–571
22. Wolterink JM, Leiner T, De Vos BD, Coatrieux JL, Kelm BM, Kondo S, Salgado RA, Shahzad R, Shu H, Snoeren M et al (2016) An evaluation of automatic coronary artery calcium scoring methods with cardiac CT using the orcascore framework. Med Phys 43(5):2361–2373
23. Callister TQ, Cooil B, Raya SP, Lippolis NJ, Russo DJ, Raggi P (1998) Coronary artery disease: improved reproducibility of calcium scoring with an electron-beam CT volumetric method. Radiology 208(3):807–814
24. Išgum I, Rutten A, Prokop M, van Ginneken B (2007) Detection of coronary calcifications from computed tomography scans for automated risk assessment of coronary artery disease. Med Phys 34(4):1450–1461
25. Brunner G, Chittajallu DR, Kurkure U, Kakadiaris IA (2010) Toward the automatic detection of coronary artery calcification in non-contrast computed tomography data. Int J Cardiovasc Imaging 26(7):829–838
26. Shahzad R, van Walsum T, Schaap M, Rossi A, Klein S, Weustink AC, de Feyter PJ, van Vliet LJ, Niessen WJ (2013) Vessel specific coronary artery calcium scoring: an automatic system. Acad Radiol 20(1):1–9
27. Long J, Shelhamer E, Darrell T (2015) Fully convolutional networks for semantic segmentation. In: Proceedings of the IEEE conference on computer vision and pattern recognition, pp 3431–3440
28. Goodfellow I, Pouget-Abadie J, Mirza M, Xu B, Warde-Farley D, Ozair S, Courville A, Bengio Y (2014) Generative adversarial nets. In: Advances in neural information processing systems, pp 2672–2680
29. Li J, Liang X, Wei Y, Xu T, Feng J, Yan S (2017) Perceptual generative adversarial networks for small object detection. In: IEEE CVPR